Accepted to EJPB, revised version

Fixed Volume Effect on Polar Properties and Phase Diagrams of Ferroelectric Semi-ellipsoidal Nanoparticles

Eugene A. Eliseev[1], Victoria V. Khist [2], Yevhen M. Fomichov[1], Maxim V. Silibin[3,4], George S. Svechnikov[5], Andrei L. Kholkin[6], Dmitry V. Karpinsky[3,7], Vladimir V. Shvartsman[8*], and Anna N. Morozovska[9†]

[1] Institute for Problems of Materials Science, National Academy of Sciences of Ukraine, 3, Krjijanovskogo, Kyiv, 03142, Ukraine,

[2]Institute of Magnetism, National Academy of Sciences of Ukraine and Ministry of Education and Science of Ukraine, Prospekt Vernadskogo 36a, 03142 Kyiv, Ukraine,

[3] National Research University of Electronic Technology "MIET", Moscow, Zelenograd, Russia,

[4]Institute for Bionic Technologies and Engineering I.M. Sechenov First Moscow State Medical University, 2-4 Bolshaya Pirogovskaya st., Moscow, Russia, 119991

[5] Sikorsky Kyiv Polytechnic Institute, Prospekt Pobedi 37, Kyiv, 03052, Ukraine

[6] Department of Physics and CICECO – Materials Institute of Aveiro, University of Aveiro, 3810-193 Aveiro, Portugal

[7] Scientific-Practical Materials Research Centre of NAS of Belarus, Minsk, Belarus

[8] Institute for Materials Science and Center for Nanointegration Duisburg-Essen (CENIDE), University of Duisburg-Essen, Universitatsstrasse 15, 45141 Essen, Germany

[9]Institute of Physics, National Academy of Sciences of Ukraine, 46, pr. Nauky, Kyiv, 03028, Ukraine

For advanced applications in modern industry, it is very important to reduce the volume of ferroelectric nanoparticles without serious deterioration of their polar properties. In many practically important cases, the fixed volume (rather than the fixed size) corresponds to realistic technological conditions of nanoparticles fabrication. The letter is focused on the theoretical study of the behavior of ferroelectric polarization, paramagnetoelectric coefficient and phase diagrams of semi-ellipsoidal nanoparticles with a fixed volume V. Our approach combines the Landau-Ginzburg-Devonshire phenomenology, the classical electrostatics, and the elasticity theory. Our results show that the size effects on the phase diagrams and polarization of semi-ellipsoidal $BiFeO_3$ nanoparticles nontrivially depend on V. These findings provide a path to optimize the polar properties of nanoparticles by controlling their phase diagrams at a fixed volume.

Keywords: semi-ellipsoidal ferroelectric nanoparticles, fixed volume, size effects, phase diagrams

* corresponding author, e-mail: vladimir.shvartsman@uni-due.de
† corresponding author, e-mail: anna.n.morozovska@gmail.com

I. INTRODUCTION

Overall miniaturization of functional ferroic materials is highly attractive for modern industry, however, the estimation of the physical properties at nanoscale level is a difficult scientific task. The resulting alteration of the physical properties with a reduction of the sample size down to a nanoscale range is currently an area of intensive study [1, 2, 3, 4]. Modern fabrication technologies for microactuators, microwave phase shifters, infrared sensors, transistor applications, energy harvesting devices, etc. need comprehensive understanding about the correlation between samples sizes and their geometry, on the one hand, and polar and magnetic order, domain sizes, domain wall thickness, and other parameters, on the other hand [1-4].

Reduction of the ferroic dimension down to a nanoscale level leads to drastic changes (including notable enhancement or suppression) of its polar, magnetic, and magnetoelectric properties. Multiple examples have been found experimentally and explained theoretically, e.g. in Rochelle salt [5, 6, 7, 8, 9], $BaTiO_3$ [10, 11, 12, 13, 14, 15], $Pb(Zr_{1-x}Ti_x)O_3$ [16, 17, 18], $KTa_{1-x}Nb_xO_3$ [19, 20, 21, 22], $SrTiO_3$ [23], and $SrBi_2Ta_2O_9$ [24, 25, 26] ferroelectric nanoparticles, as well as for pristine [27, 28, 29, 30, 31] and rare-earth doped [32, 33, 34, 35, 36, 37] $BiFeO_3$ multiferroic nanoparticles, nanograins, nanoislands [38], and their self-assembled arrays [39, 40, 41].

$BiFeO_3$ based materials continue to attract significant scientific interest due to the number of phase transitions and related changes in the unique multiferroic properties under different stimuli such as chemical doping, pressure, temperature and radiation [42, 43, 44, 45, 46, 47, 48, 49]. However, most studies [27, 29-41] of the size-dependent properties of nanosized ferroelectric antiferromagnet $BiFeO_3$ unequivocally show the decrease of polar and antifferomagnetic transition temperatures with a reduction of grain size; e.g. the Neel transition temperature is around 550 K for (10 – 5) nm $BiFeO_3$ grains [27] (in comparison with 650 K for a bulk sample). Pronounced effects on the remanent polarization, dielectric permittivity, coercive field, and ferroelectric phase transition temperature have also been observed for $BiFeO_3$ nanoparticles with effective grain sizes below 50 nm [50, 51, 52]. All these results suggest that at the nanoscale level the properties of $BiFeO_3$ are exceptional and complex. In spite of a number of studies devoted to size effects on physical properties of $BiFeO_3$-based materials [27, 29-41] there is no self-consistent model describing the evolution of the polarization as a function of grain volume in the nanoscale range for different grain geometries.

Recently [29] the size effects on phase diagrams, ferroelectric, and magnetoelectric properties of semi-ellipsoidal $BiFeO_3$ nanoparticles clamped to a rigid conductive substrate have been studied using the Landau-Ginzburg-Devonshire (LGD) phenomenology [53, 54]. Nanoparticles of semi-ellipsoidal shape are considered as model objects to study size effects on physical properties of ferroic

nano-islands. $BiFeO_3$ nano-islands and their self-assembled arrays can be formed on anisotropic substrates by different low-damage fabrication methods [39, 40, 41].

The above state-of-art analyses motivated us to conduct a theoretical study of the size effects on ferroelectric properties of semi-ellipsoidal $BiFeO_3$ nanoparticles under a fixed volume condition [**Fig. 1**] corresponding to realistic experiments [39, 40, 41]. We have used LGD phenomenology combined with the classical electrostatics and elasticity theory.

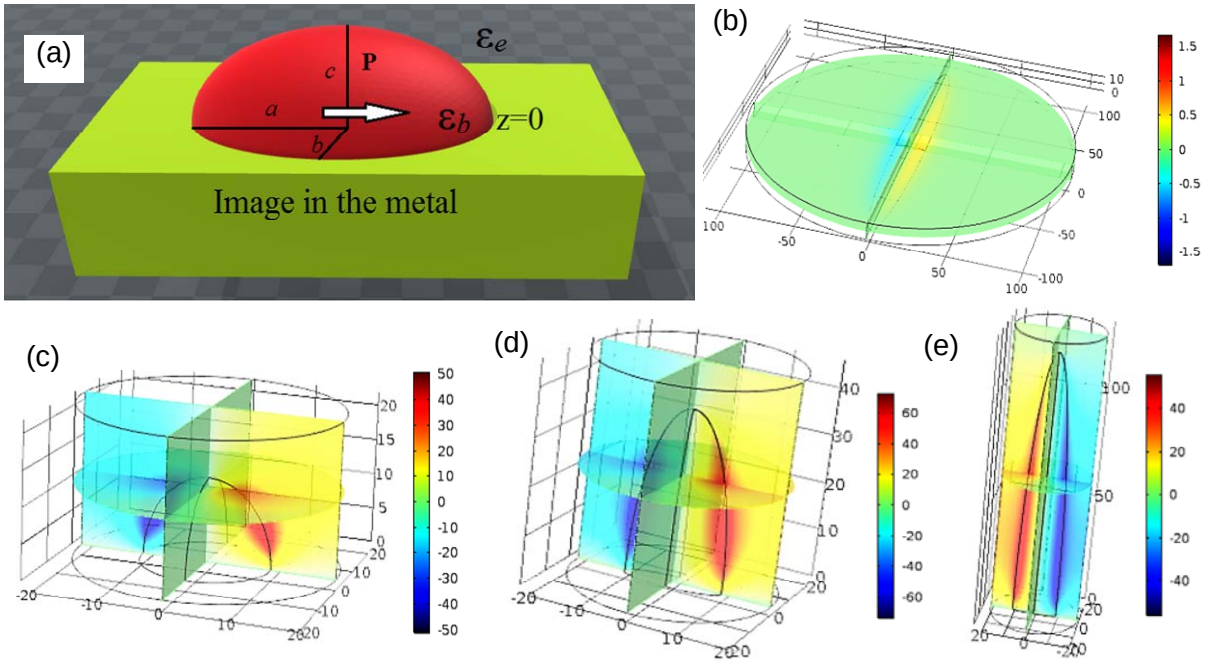

FIG. 1. (a) Semi-ellipsoidal uniformly polarized ferroelectric nanoparticles are clamped to a rigid conducting substrate electrode. The one-component ferroelectric polarization $\mathbf{P}(\mathbf{r})$ is directed along the X-axes**.** Semi-ellipsoid height is denoted by *c* and lateral semi-axes by *a* and *b*, respectively. Parts **(b)-(e)** show the electric potential distribution inside the particles, which have different aspect ratios a/b=0.1, 1, 3, 10 and the same volume. The color scale is in Volts.

II. PROBLEM STATEMENT AND BASIC EQUATIONS

A. Basic equations and analytical expressions

We consider ferroelectric nanoparticles in the form of semi-elliptical islands precipitated on a rigid conducting substrate electrode. The ellipsoid has different values of semi-axis length, *a*, *b* and *c* along the X-, Y- and Z-axis, respectively [see **Fig. 1(a)**]. The sizes can vary, while the particle volume $V=(2/3)\pi abc$ is fixed to satisfy technological conditions of the nanoparticle preparation by e.g. laser ablation. We denote ε_b and ε_e as the isotropic dielectric permittivity of the ferroelectric background [55] and external media, respectively. Dependences of the *x*- and *y*-components of the electric polarizations on the electric field **E** are linear, $P_{y,z}=\varepsilon_0(\varepsilon_b-1)E_{y,z}$, and the polarization *x*-component

contains the ferroelectric (P) and background ($\sim E_x$) contributions, $P_x = P + \varepsilon_0(\varepsilon_b - 1)E_x$, where ε_0 is the universal dielectric constant. The ferroelectric contribution, $P(\mathbf{r}, E_3)$, was determined from the minimization of 2-4-power expansion of the LGD free energy leading to the equation inside a nanoparticle [29],

$$\alpha P + \beta P^3 - g_{33mn}\frac{\partial^2 P}{\partial x_m \partial x_n} = E_x, \qquad (1)$$

where the coefficient $\alpha(T) = \alpha_T(T - T_C)$, α_T is the inverse Curie-Weiss constant, T is the absolute temperature, and T_C is the bulk Curie temperature of the paraelectric-to-ferroelectric phase transition. The parameter $\beta>0$ is the coefficient of LGD potential expansion on the polarization powers for ferroelectrics with the second-order phase transition to a paraelectric phase. Boundary conditions for the polarization P_x at the particle surface S are regarded to be natural, $(\partial P_x/\partial \mathbf{n})|_S = 0$.

The electric field E_i is defined via the electric potential as $E_i = -\partial\varphi/\partial x_i$. For a ferroelectric particle without free charges, the electric potential φ can be found self-consistently from the Laplace equation outside the nanoparticle ($\varepsilon_0\varepsilon_e\Delta\varphi = 0$) and Poisson equation inside the nanoparticle ($\varepsilon_0\varepsilon_b\Delta\varphi = \partial P/\partial x$). The corresponding electric boundary conditions are the continuity of the potential at the particle surface S, $(\varphi_e - \varphi_i)|_S = 0$, and the difference of normal components of electric displacements, which is equal to the surface screening charge density at the particle surface S, $(\mathbf{D}_e - \mathbf{D}_i)\mathbf{n} + \varepsilon_0\left.\frac{\varphi_i}{\lambda}\right|_S = 0$, where $\mathbf{D}_i = \varepsilon_0\varepsilon_b\mathbf{E}_i + \mathbf{P}$ inside the particle and $\mathbf{D}_e = \varepsilon_0\varepsilon_e\mathbf{E}_e$ outside the particle; λ is the surface screening length. The subscript "i" corresponds to the electric field or potential inside the particle and "e" – outside the particle. The potential is constant at the particle-electrode interface, i.e. $\varphi_i|_{z=0} = 0$.

Notably the electrostriction effect does not contribute significantly to the results neither of this work, nor to the results presented in Ref.[29], because we regard that internal stresses σ_{kl} are absent for a nanoparticle base placed on an elastically matched substrate and with a mechanically-free semi-ellipsoid surface. Actually when the electrostrictive term $2Q_{kli3}\sigma_{kl}P_3$ is included in Eq.(1) it renormalizes the coefficient α as $\alpha \to \alpha - 2Q_{kli3}\sigma_{kl}$, where Q_{kli3} are electrostriction tensor components.

We calculated the spatial distribution and the average electric field inside the $BiFeO_3$ particles using finite element modeling (FEM) with the material parameters listed in **Table I**. The parameters of $BiFeO_3$ are collected from Refs.[42-49, 29].

Table I. Parameters of bulk $BiFeO_3$ used in our calculations

Parameter	SI units	Value for $BiFeO_3$
Spontaneous polarization P_S	C/m^2	1
Electrostriction coefficient Q_{12}	m^4/C^2	–0.016
Electrostriction coefficient Q_{11}	m^4/C^2	+0.032
Background permittivity ε_b	dimensionless	10
Ambient permittivity ε_e	dimensionless	1
Gradient coefficient g_{11}	m^3/F	10^{-10}
Gradient coefficient g_{44}	m^3/F	10^{-9}
LGD coefficient β	$J\ m^5/C^4$	10^7
LGD coefficient α	m/F	-10^7 (at 300 K)
Ferroelectric Curie temperature T_c	K	1100
Temperature coefficient α_T	m/(K·F)	0.9×10^6
Antiferromagnetic Neel temperature	K	650
Surface screening length λ	nm	10^{-3} to 10^2
Universal dielectric constant ε_0	F/m	8.85×10^{-12}

By analyzing the FEM results in Ref. [29] we derived a sufficiently accurate analytical expression for the transition temperature from the ferroelectric (FE) to the paraelectric (PE) phase $T_{cr}(a,b,c)$:

$$T_{cr}(a,b,c) = T_C - \frac{n_d(a,b,c)}{\alpha_T \varepsilon_0}. \tag{2}$$

The effective depolarization factor $n_d(a,b,c)$ in Eq.(2) depends on the semi-ellipsoid geometry as listed in Ref. [29]. The average spontaneous polarization that is nonzero in the temperature range $T < T_{cr}(a,b,c)$,

$$P_S = \sqrt{\frac{\alpha_T}{\beta}\left(T_{cr}(a,b,c) - T\right)}. \tag{3}$$

The sizes *a, b* and *c* are related by the fixed volume condition, $V = (2/3)\pi abc$, i.e. only 2 of them can be varied independently in expressions (2)-(3). Rewriting the expressions for $n_d(a,b,c)$ from Ref. [29] vs. the volume $V = (2/3)\pi abc$ and the ratio $a/b = \gamma$, we get that $c = \frac{3V\gamma}{2\pi a^2}$ and so

$$n_d(a,V,\gamma) = \frac{\lambda n_\infty(a,V,\gamma)}{\lambda + R(a,V,\gamma) n_\infty(a,V,\gamma)}, \tag{4}$$

$$R \approx a\left(0.62 + 0.19\gamma + 0.52\frac{a^3}{V}\frac{1}{\gamma}\right), \tag{5}$$

$$n_\infty \approx \frac{1}{(\varepsilon_b + \varepsilon_e\gamma)}\left(1 + 0.4\frac{a^3}{V}\frac{1}{\gamma} + \left(\frac{2\pi a^3}{3V}\right)^2 \frac{1}{\gamma^3 + 0.075\gamma^4}\right)^{-1}. \tag{6}$$

The physical meaning of n_∞ is the "bare" depolarization factor of the nanoparticle for $\lambda \to \infty$ corresponding to the absence of surface screening [29].

B. Conditions of the single-domain state stability in semi-ellipsoidal nanoparticles

According to numerical results for thin ferroelectric $PbTiO_3$ films [56, 57] and $CuInP_2S_6$ nanoparticles [58], the stability of a single-domain state in comparison with a poly-domain state and a paraelectric phase depends on a balance between the depolarization field energy (appearing from incomplete screening of the spontaneous polarization by surface charges with finite screening length λ) and the domain walls energy that is proportional to the gradient coefficient g_{44} and the domain walls area. According to additional numerical calculations and analytical estimations performed in this work the domain splitting starts when it becomes energetically preferable. At the threshold of the domain formation the single-domain (SD) state energy excess G_{SD} that includes the electrostatic energy and Landau-Ginzburg-Devonshire contributions of a homogeneously polarized nanoparticle, $G_{el} = -\int_V d^3r \frac{P_x E_x}{2} - \int_S d^2r \left(\frac{\varepsilon_0 \varphi^2}{2\lambda} \right)$ and $G_{LGD} = \int_V d^3r \left(\frac{\alpha}{2} P_x^2 + \frac{\beta}{4} P_x^4 \right)$, respectively, becomes equal to the energy of a particle with domain walls, $G_{PD} = G_{LGD} + G_{el} + G_g$. The introduced gradient energy $G_g = \int_V d^3r \left(\frac{g_{11}}{2} \left(\frac{\partial P_x}{\partial x} \right)^2 + \frac{g_{44}}{2} \left[\left(\frac{\partial P_x}{\partial y} \right)^2 + \left(\frac{\partial P_x}{\partial z} \right)^2 \right] \right)$ is formally equal to the energy of the domain walls, $G_S = \psi_S S_{DW}$, where ψ_S is the surface energy of the domain wall and S_{DW} is the area of the domain wall. ψ_S is related with the LGD coefficients as $\psi_S = \frac{2\sqrt{-2\alpha^3 g_{44}}}{3\beta}$ [59].

Hence expressions for the SD state energy excess G_{SD} and domain walls energy G_S are

$$G_{SD} = -\frac{\alpha_R^2}{4\beta} V, \qquad G_S = \frac{2\sqrt{-2\alpha_R^3 g_{44}}}{3\beta} S_{DW}. \tag{7}$$

Here the coefficient $\alpha_R = \alpha_T \left(T - T_{cr}(a,b,c) \right)$, transition temperature $T_{cr}(a,b,c) = T_C - \frac{n_d(a,b,c)}{\alpha_T \varepsilon_0}$, semi-ellipsoid volume $V = \frac{2\pi}{3} abc$, and domain wall area of the full cross-section $S_{DW} = \pi ab$ (for $b < c$) or $S_{DW} = \pi ac$ (for $b > c$). The single-domain state and the two-domain state with a domain wall dividing the particle into two equal parts are shown in **Fig.2(a)** and **2(b)**, respectively.

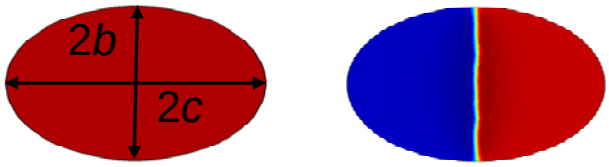

(a) single-domain (b) two-domain

FIG. 2. Polarization distributions in the y-z cross-section of the semi-ellipsoidal nanoparticle with height a=10 nm, λ=0.1 nm, $g_{44}=10^{-10}$ m^3/F and room temperature. Cross-section **(a)** shows the single-domain state and **(b)** two-domain state**.** Other parameters are listed in **Table I.**

In accordance with Virial's theorem the equality $G_D = -2G_S$ leads to the equation $\sqrt{-\alpha_R}\,\frac{c}{8} = \sqrt{2g_{44}}$, that in turn leads to the expression for the critical gradient coefficient at fixed temperature T and screening length λ, is $g_{44}^{cr} = -\alpha_R \frac{c^2}{128} \equiv -\frac{c^2}{128}\alpha_T\left(T - T_{cr}(a,b,c)\right)$, or in the explicit form:

$$g_{44}^{cr} = \frac{c^2}{128}\alpha_T\left(T_{cr}(a,b,c) - T\right) \equiv \frac{c^2}{128}\alpha_T\left(T_C - \frac{n_d(a,b,c)}{\alpha_T \varepsilon_0} - T\right). \qquad (8)$$

The domain formation starts if $g_{44} < g_{44}^{cr}$ and the single-domain state is stable at $g_{44} > g_{44}^{cr}$.

Using the numerical values from **Table I**, $c \le 10$ nm, $\alpha_T = 0.9\times10^6$ m/(K·F), $T_C = 1100$ K, $\varepsilon_0 = 8.85\times10^{-12}$ F/m, $a/\lambda \ge 10^3$, $\varepsilon_b = 10$, and approximation for $n_d \approx \frac{\lambda n_\infty}{\lambda + 0.62 a n_\infty}$ and $n_\infty \approx \frac{1}{(\varepsilon_b + \varepsilon_e \gamma)}$, we estimated that $g_{44}^{cr} \le \frac{c^2}{128}\alpha_T\left(T_C - T\right) \le 7\times10^{-10}$ m^3/F at room temperature. Additional numerical simulation assured us that the single domain state is mostly stable for the parameters listed in **Table I.**

III. SIZE EFFECTS OF POLARIZATION AND PHASE DIAGRAMS AT FIXED VOLUME

Figure 3 shows the phase diagram of semi-ellipsoidal $BiFeO_3$ nanoparticles. *Y*-axis is the relative temperature T/T_C and X-axis is the nanoparticle volume *V*. Different curves are calculated for several values of the aspect ratio a/b =0.1, 1 3, 10. The boundary between paraelectric (**PE**) and ferroelectric (**FE**) phases, given by the critical temperature of the size-induced phase transition $T_{cr}(a,b,c)$, monotonously increases with the increasing a/b ratio. The size effect manifests itself in the ferroelectricity disappearance at a critical volume $V_{cr}(a,b)$, for which $T_{cr} = 0$, and in the monotonous

increase of the transition temperature with the increasing volume, followed by its further saturation to T_C for $V > 10^8$ nm^3.

The series of curves in **Fig. 3** show the influence of the particle volume V and the aspect ratio a/b (proportional to the size a in the direction of spontaneous polarization) on the ferroelectric phase transition. The transition temperature monotonically increases and the critical volume V_{cr} decreases with the increasing a/b ratio (see the sequence of black, red, blue, and magenta curves). At the minimal a/b ratio the phase transition occurs at the largest value of V (see the black curve). This is due to the influence of the depolarization field directed along the x-axis, which is maximal for the smallest a-size. The higher is the aspect ratio a/b, the smaller is the depolarization field, and hence the higher the transition temperature and the smaller the critical size. For the maximal value of a/b, the phase transition occurs at the smallest value of V (see the magenta curve). It should also be noted that the critical volume for this curve is less than 1 nm^3, which lies beyond the limits of continuous theory applicability (every size should be at least one order of magnitude greater that the lattice constant ~ 0.4 nm).

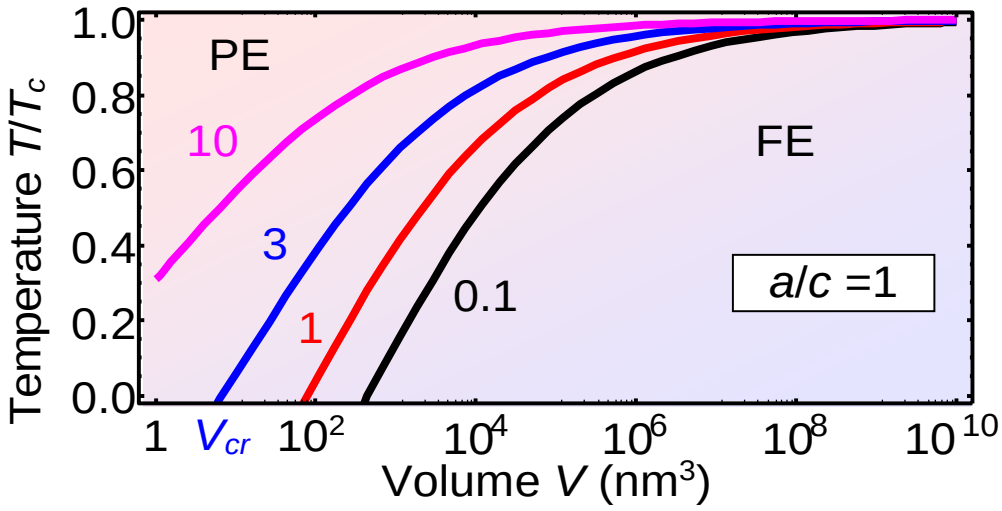

FIG. 3. Phase diagrams of $BiFeO_3$ nanoparticle in coordinates "temperature T – volume of semi-ellipsoidal particle V" calculated for the fixed aspect ratio a/c=1 and the different aspect ratios a/b=0.3, 1, 3, 10 (see numbers near the curves) and the screening length λ=0.1 nm.

Phase diagrams of a semi-ellipsoidal $BiFeO_3$ nanoparticles in the coordinates: "relative temperature T/T_C " and "length of the particle semi-axis a", are shown in **Figs.4(a)-(c)** for the fixed particle volume $V = 5\times10^3$, 5×10^4 and 5×10^6 nm^3, respectively. Different curves on each panel are calculated for several values of the aspect ratio a/b=0.1, 1, 3, 10. The ferroelectricity disappearance at

the critical size $a_{cr}(b,c)$, for which $T_{cr}=0$, is followed by the monotonic increase of the transition temperature with the increasing size a and its further saturation to T_C for the sizes $a>(50-100)$ nm.

We found that the boundary between the PE and FE phases nontrivially depends on the aspect ratio a/b. Comparison between the curves in plots **4(a) – 4(c)** calculated for the fixed V shows that the phase diagram is the most nontrivial for V=5×10^3 nm^3, where there are multiple intersections of the curves calculated for different aspect ratios a/b. One intersection of the curve for a/b=10 (magenta curve) and a/b=0.1 (black curve) corresponds to $a \approx 5$ nm. Another intersection of the curves calculated for a/b=0.1 (black curve) and a/b=3 (blue curve) takes place at $a \approx 5$ nm. The curve for a/b=1 (red) intersects the curve for a/b=3 (blue) at $a \approx 10$ nm, and the curve for a/b=10 at $a \approx 13$ nm. The shape of the curves for V=5×10^4 nm^3 is qualitatively the same as for V=5×10^3 nm^3, but differs quantitatively, because the smallest semi-axes length, when an intersection occurs between the transition line for a/b=0.1 (black curve) with the curves for other particle aspect ratio, is $a \approx 8$ nm.

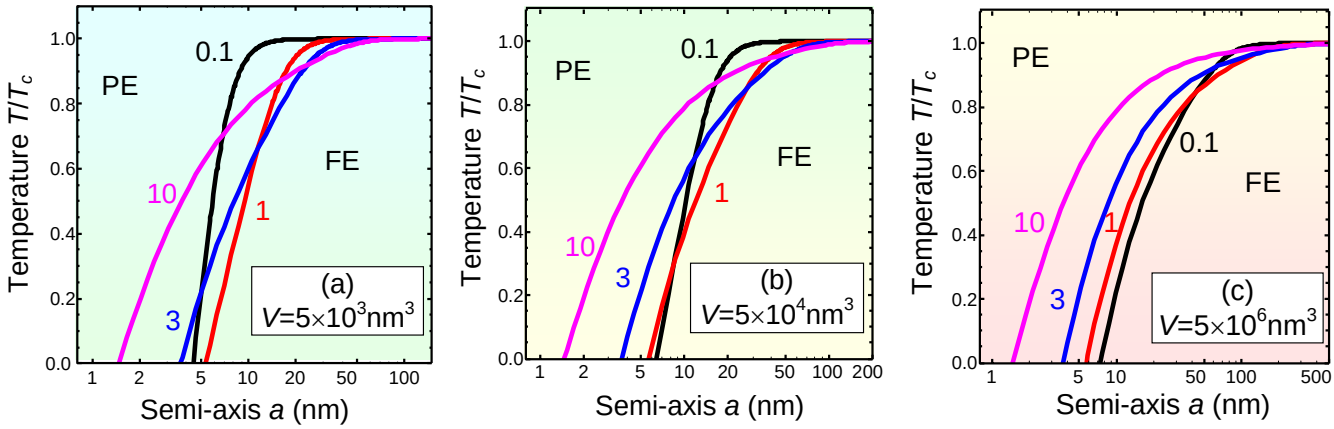

FIG. 4. Phase diagrams of $BiFeO_3$ nanoparticles in the coordinates "temperature – length of ellipsoid semi-axis a", calculated at the fixed volume V=5×10^3 nm^3 **(a),** V=5×10^4 nm^3 **(b),** and V=5×10^6 nm^3 **(c),** for the different aspect ratios a/b=0.1, 1, 3, 10 (see numbers near the curves) and the screening length λ=0.1 nm.

The transition lines corresponding to the different a/b values intersect at all chosen values of V but the intersections are separated better at small volumes [compare **Figs. 4(a), (b)** and **(c)**]. This result is nontrivial and important, since the appearance of such intersections can affect the optimization procedure of the nanoparticles polar properties at a fixed volume, thus being useful for the potential applications of $BiFeO_3$.

Hence it is important to explain the origin of the intersections. Based on the analytical expressions (2)-(6), we conclude that the transition temperatures can be the same for different sizes

a,b,c of the particle, if only the effective depolarization factor $n_d(a,b,c)$ given by Eq.(4) is an ambiguous function of the sizes at the fixed volume V. Elementary calculations show that $n_d(a,V,\gamma)$ in Eq.(4) is an ambiguous function of a and γ at fixed V.

Spontaneous polarization dependences on the length of ellipsoid semi-axis a calculated for the fixed particle volume $V = 5\times10^3$, 5×10^4, and 5×10^6 nm^3 at room temperature are shown in **Figs. 5(a), (b)** and **(c)**, respectively**.** The curves in the each panel are calculated for several values of the aspect ratio a/b =0.1, 1, 3, 10 and the fixed particle volume V. The spontaneous polarization appears at the critical size $a_{cr}(a,V)$ and increases with size a for all a/b ratios. The critical size decreases with the increase of the a/b ratio. The spontaneous polarization saturates to the bulk value ~ 1 C/m^2 at sizes $a > 50$nm. Note that the polarization of the nanoparticles with a/b = 10 saturates slower than that of the particles with a/b = 0.1. Hence the saturation rate increases with the decreasing a/b, as can be observed from **Figs. 5(a)-(c)**. The polarization curves have intersection points for a/b =0.1 and a/b =3 at a=5 nm [**Fig. 5 (b)**]; the curves for a/b =0.1 and a/b =1 also intersect at a≈8 nm. Hence the comparison of the curves order shown in **Figs 5** allows us to state that the dependence of the nanoparticle polarization on the semi-ellipsoid a-axis length for V=5×10^3 nm^3 is unusual due to the mixed order of different curves and their intersections at small sizes, whereas for V=5×10^6 nm^3 the curves order is expected with increasing a/b, and the intersections can appear for long semi-axes only (compare with the diagrams shown in **Figs.4**). The phase transition for the highest aspect ratio a/b =10 occurs at the minimum value of a (see the magenta curve). The phase transition for the smallest ratio a/b = 0.1 (see the black curve) corresponds to the maximal value of a.

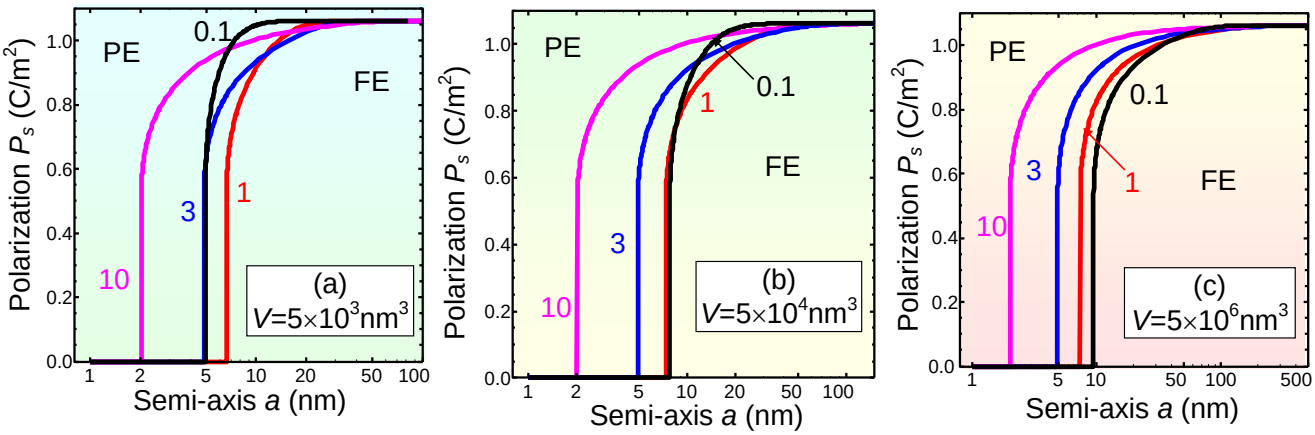

FIG. 5. The spontaneous polarization dependences on the length of ellipsoid semi-axis a calculated at room temperature (300 K), fixed volume V=5×10^3 nm^3 **(a),** V=5×10^4 nm^3 **(b)** and V=5×10^6 nm^3 **(c)** for the different

aspect ratios a/b =0.1, 1, 3, 10 (see numbers near the curves). The screening length λ=0.1 nm, T=300 K; other parameters correspond to bulk $BiFeO_3$.

IV. PARAMAGNETOELECTRIC (PME) COEFFICIENT AT FIXED VOLUME

In multiferroic magnetoelectric materials, like $BiFeO_3$, besides of the linear and biquadratic couplings of magnetic and electric order parameters [42, 28], linear-quadratic paramagnetoelectric (**PME**) effect should exist in the paramagnetic phase below the T_C temperature of the paraelectric-to-ferroelectric phase transition, where the electric polarization is non-zero. This effect was first observed in piezoelectric paramagnetic crystal $NiSO_4 \cdot 6H_2O$ [60]. It was later measured in Mn-doped $SrTiO_3$ [61], magnetoelectric multiferroic $Pb(Fe_{1/2}Nb_{1/2})O_3$ (PFN) [62, 63, 64], and metal-organic framework [65].

Below we consider only the PME effect at a fixed volume, which exists even in a paramagnetic phase and is insensitive to the magnetic symmetry changes in nanoparticles. As it has been shown in Refs. [66, 67] the PME coefficient η is proportional to the biquadratic magnetoelectric coupling (ME) coefficient ξ_{MP} that couples the second powers of polarization and magnetic order parameters, the average spontaneous polarization $P_S(T)$ given by Eq.(3), linear dielectric susceptibility, $\chi_{FE}(T)$, and square of the magnetic susceptibility, $\chi_M(T)$ [29]:

$$\eta(T) = -P_S(T)\chi_{FE}(T)(\chi_M(T))^2\ \xi_{MP} \equiv \begin{cases} \dfrac{-\xi_{MP}(\chi_M(T))^2}{2\sqrt{\alpha_T \beta (T_{cr}(a,b,c) - T)}}, & T < T_{cr}, \\ 0, \quad T > T_{cr}. \end{cases} \qquad (9)$$

Approximate expression for the magnetic susceptibility is taken the same as in Ref. [29], $\chi_M(T) = \dfrac{\mu_0}{\alpha_M^{(T)}(T-\theta) + \xi_{LM}L^2 + \xi_{MP}P_S^2(T)}$. Equation (9) is valid in the FE-AFM phase (with nonzero AFM long-range order parameter $L \neq 0$) as well as in the paramagnetic FE phase without any magnetic order at L=0. Parameters ξ_{LM} and ξ_{MP} are the biquadratic ME coefficients, which couple with the second powers of polarization and magnetic order parameters in the ME energy.

Dependences of the PME coefficient on the volume of the half ellipsoid, V, calculated at room temperature (T = 300 K) for various values of the half-ratio a/b are shown in **Fig. 6.** The length of the other semi-axis, c, is chosen from the formula $c = 3V/(4\pi ab)$ (see different curves calculated for a/b = 0.1, 2, 3, 10). The PME coefficient is normalized to the bulk value. The PME coefficient is zero for sizes $a < a_{cr}(b,c)$ due to disappearance of the spontaneous polarization, it appears at $a > a_{cr}$ and diverges at a critical value $a = a_{cr}(b,c)$, then it decreases with increasing a. The PME coefficient reaches a bulk value at sizes $a >> 100$ nm. The divergence at $a = a_{cr}(b,c)$ demonstrates the possibility

of obtaining a giant PME effect in $BiFeO_3$ nanoparticles near the size-induced transition from the FE phase to PE phase, in particular, the normalized PME coefficient substantially exceeds 1 for sizes $a_{cr}(b,c) \le a < 2a_{cr}(b,c)$. Note that the PME coefficient at $V = 5\times10^3$ nm^3 achieves saturation significantly faster than at $V = 5\times10^6$ nm^3 [compare the curves in **Figs.6(a) - 6(c)**]. The PME curves calculated for different volumes are very close to each other at $V = 10^2$ nm^3 and are well separated from each other at $V = 5\times10^6$ nm^3.

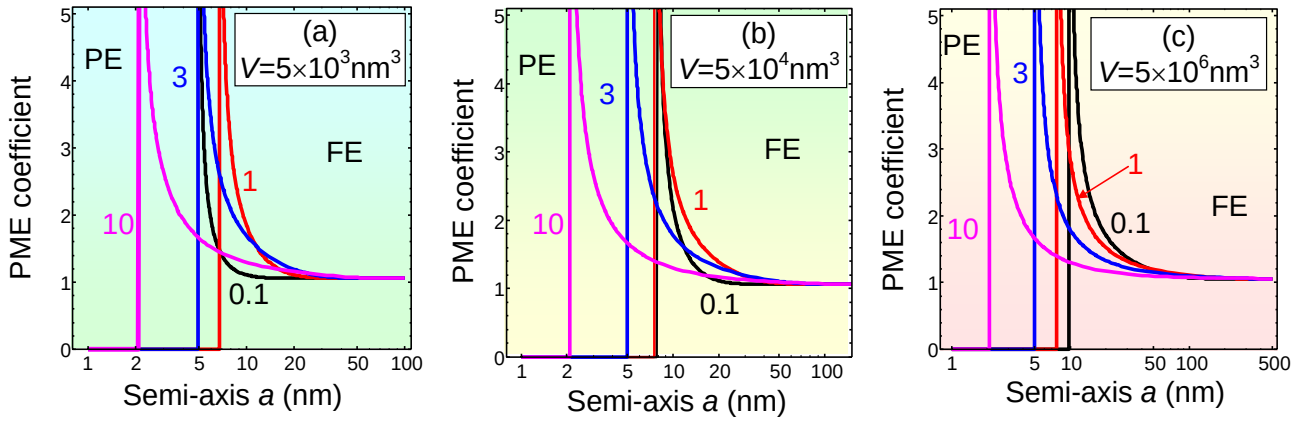

FIG. 6. The PME coefficient dependences on the length of ellipsoid semi-axis a calculated at room temperature (300 K), the fixed volume V=5×10^3 nm^3 **(a),** V=5×10^4 nm^3 **(b)** and V=5×10^6 nm^3 **(c)** for the different aspect ratios a/b =0.1, 1, 3, 10 (see numbers near the curves). The screening length λ=0.1 nm, T=300 K; other parameters correspond to bulk $BiFeO_3$.

The comparative analysis of **Fig. 6 (a) - (c)** confirms our conclusion that the size effects for the spontaneous polarization and PME coefficient are sensitive to the ratio bc/a^2 in the direction of the polarization for a given volume and are less sensitive to the absolute size of the nanoparticles.

V. CONCLUSION

To resume, using a combination of the Landau-Ginzburg-Devonshire phenomenology, classical electrostatics, and elasticity theory, we have studied the size effect on the phase diagrams and ferroelectric polarization of semi-ellipsoidal $BiFeO_3$ nanoparticles with three different semi-axes and fixed volume V. The fixed volume condition corresponds to realistic technological conditions of nanoparticle fabrication [39-41]. Our analysis utilizes the analytical expressions derived in the earlier study [29] for the dependence of the ferroelectric transition temperature, average polarization, and PME coefficient on the particle size, and here we account for the fact that the product of the particle's semi-axes abc is fixed, since the semi-ellipsoid volume is $V = (2/3)\pi abc$. The analyses of the obtained results leads to the conclusion that the size effects of the phase diagrams and polarization

nontrivially depend on the particle volume V and aspect ratio in the polarization direction, a/b. These results open the way to control the properties and govern phase diagrams under the realistic experimental conditions of fixed particle volume.

ACKNOWLEDGMENTS. This project has received funding from the European Union's Horizon 2020 research and innovation programme under the Marie Skłodowska-Curie grant agreement No 778070. M.V.S. and D.V.K acknowledge MK-1720.2017.8, RFFI (#17-58-45026). A.L.K. acknowledges support from CICECO-Aveiro Institute of Materials (Ref. FCT UID/CTM/50011/2013), financed by national funds through the FCT/MEC and when applicable co-financed by FEDER under the PT2020 Partnership Agreement. A.N.M. work was partially supported by the National Academy of Sciences of Ukraine (projects No. 0117U002612 and No. 0118U003375)

Authors' contribution. E.A.E. performed numerical calculations and, jointly with V.V.K. and Y.M.F., generated figures. M.V.S., G.S.S., A.L.K., D.V.K. and V.V.S. worked on results interpretation and discussion. A.N.M. generated the research idea, stated the problem, made analytical estimates and wrote the manuscript. V.V.S. worked on the manuscript improvement.

REFERENCES

1 J.F. Scott Ferroelectric Memories [Springer Series in Advanced Microelectronics: Vol. 3] / J.F. Scott. - Springer Verlag, 2000- 248 p. - ISBN: 978-3-540-66387-4.

2 D.R. Tilley Finite-size effects on phase transitions in ferroelectrics. Ferroelectic Thin Films. ed. C. Paz de Araujo, J.F.Scott and G.W. Teylor.-Amsterdam: Gordon and Breach, 1996.-P.11-4

3 A.K. Tagantsev, L. E. Cross, and J. Fousek. Domains in ferroic crystals and thin films. New York: Springer, 2010. ISBN 978-1-4419-1416-3, e-ISBN 978-1-4419-1417-0, DOI 10.1007/978-1-4419-1417-0

4 M.D. Glinchuk, A.V. Ragulya, V.A. Stephanovich. Nanoferroics. Dordrecht: Springer; 2013 May 13., p.378

5. D. Yadlovker, S. Berger, Uniform orientation and size of ferroelectric domains, Phys. Rev. B. 71, 184112-1-6 (2005).

6. D. Yadlovker, S. Berger, Reversible electric field induced nonferroelectric to ferroelectric phase transition in single crystal nanorods of potassium nitrate, Appl. Phys. Lett. 91, 173104 (2007).

7. D. Yadlovker, S. Berger, Nucleation and growth of single crystals with uniform crystallographic orientation inside alumina nanopores, J. Appl. Phys. 101, 034304 (2007).

8 A.N. Morozovska, E.A. Eliseev, M.D. Glinchuk. Size effects and depolarization field influence on the phase diagrams of cylindrical ferroelectric nanoparticles. Physica B 387, № 1-2, 358–366 (2007).

9 A.N. Morozovska, M.D. Glinchuk, E.A. Eliseev. Phase transitions induced by confinement of ferroic nanoparticles. Phys. Rev. B 76 014102-1-13 (2007).

10. M. H. Frey, D. A. Payne, Grain-size effect on structure and phase transformations for barium titanate, Phys. Rev. B 54, 3158- 3168 (1996).

11. Z. Zhao, V. Buscaglia, M. Viviani, M.T. Buscaglia, L. Mitoseriu, A. Testino, M. Nygren, M. Johnsson, P. Nanni, Grain-size effects on the ferroelectric behavior of dense nanocrystalline $BaTiO_3$ ceramics, Phys. Rev. B 70, 024107-1-8 (2004).

12 A.N. Morozovska and M.D. Glinchuk. Reentrant phase in nanoferroics induced by the flexoelectric and Vegard effects. J. Appl. Phys. 119, 094109 (2016).

13 M.D. Glinchuk, E.A. Eliseev, A.N. Morozovska. Superparaelectric phase in the ensemble of noninteracting ferroelectric nanoparticles. Phys. Rev. B. 78, 134107-1-9 (2008).

14. P. Perriat, J. C. Niepce, G. Caboche, Thermodynamic considerations of the grain size dependency of material properties: a new approach to explain the variation of the dielectric permittivity of $BaTiO_3$ with grain size, J. Therm. Anal. Calorim. 41, 635-649 (1994).

15. M. Wenhui, Surface tension and Curie temperature in ferroelectric nanowires and nanodots, Appl. Phys. A 96, 915–920 (2009).

16. E. Erdem, H.-Ch. Semmelhack, R. Bottcher, H. Rumpf, J. Banys, A.Matthes, H.-J. Glasel, D. Hirsch, E. Hartmann, Study of the tetragonal-to-cubic phase transition in $PbTiO_3$ nanopowders, J. Phys.: Condens. Matter 18, 3861–3874 (2006).

17. H. Huang, C. Q. Sun, P. Hing, Surface bond contraction and its effect on the nanometric sized lead zirconate titanate. J. Phys.: Condens. Matter 12, L127–L132 (2000).

18. H. Huang, C. Q. Sun, Z. Tianshu, P. Hing, Grain-size effect on ferroelectric $Pb(Zr_{1-x}Ti_x)O_3$ solid solutions induced by surface bond contraction. Phys. Rev. B 63, 184112 (2001).
19 I.S. Golovina, S.P. Kolesnik, V. Bryksa, V.V. Strelchuk, I.B. Yanchuk, I.N. Geifman, S.A. Khainakov, S.V. Svechnikov, A.N. Morozovska, Defect driven ferroelectricity and magnetism in nanocrystalline $KTaO_3$, Physica B 407, 614-623 (2012).
20 I.S. Golovina, V.P. Bryksa, V.V. Strelchuk, I.N. Geifman, A.A. Andriiko, Size effects in the temperatures of phase transitions in $KNbO_3$ nanopowder. J. Appl. Phys. 113, 144103 (2013).
21. I.S. Golovina, V.P. Bryksa, V.V. Strelchuk, I.N. Geifman, Phase transitions in the nanopowders $KTa_{0.5}Nb_{0.5}O_3$ studied by Raman spectroscopy. Funct. Mater. 20, 75-80 (2013).
22 A.N. Morozovska, I.S. Golovina, S.V. Lemishko, A.A. Andriiko, S.A. Khainakov, and E.A. Eliseev. Effect of Vegard strains on the extrinsic size effects in ferroelectric nanoparticles. Phys. Rev. B 90, 214103 (2014).
23 E.A. Eliseev, A.N. Morozovska, M.D. Glinchuk, and R. Blinc. Anion vacancy-driven magnetism in incipient ferroelectric $SrTiO_3$ and $KTaO_3$ nanoparticles. J. Appl. Phys. 109, 094105 (2011).
24. T. Yu, Z. X. Shen, W. S. Toh, J. M. Xue, J. Wang, Size effect on the ferroelectric phase transition in $SrBi_2Ta_2O_9$ nanoparticles. J. Appl. Phys. 94, 618 (2003).
25. H. Ke, D. C. Jia, W. Wang, Y. Zhou, Ferroelectric phase transition investigated by thermal analysis and Raman scattering in $SrBi_2Ta_2O_9$ nanoparticles. Solid State Phenomena 121-123, 843-846 (2007).
26 E.A.Eliseev, A.V.Semchenko, Y.M.Fomichov, M. D. Glinchuk, V.V.Sidsky, V.V.Kolos, Yu.M.Pleskachevsky, M.V.Silibin, N.V.Morozovsky, A.N.Morozovska. Surface and finite size effects impact on the phase diagrams, polar and dielectric properties of $(Sr,Bi)Ta_2O_9$ ferroelectric nanoparticles. J. Appl. Phys. 119, 204104 (2016).
27 S. Goswami, D. Bhattacharya, P. Choudhury. Particle size dependence of magnetization and noncentrosymmetry in nanoscale $BiFeO_3$. J. Appl. Phys. 109, 07D737 (2011).
28 M.D. Glinchuk, E.A. Eliseev, A.N. Morozovska, R. Blinc. Giant magnetoelectric effect induced by intrinsic surface stress in ferroic nanorods. Phys. Rev. B 77, 024106-1-11 (2008).
29 V.V. Khist, E.A. Eliseev, M.D. Glinchuk, D.V. Karpinsky, M.V. Silibin, and A.N. Morozovska. Size Effects of Ferroelectric and Magnetoelectric Properties of Semi-ellipsoidal Bismuth Ferrite Nanoparticles. J. Alloys Compd., 714, 15, 303–310 (2017).
30. S. Layek and H. C. Verma, Magnetic and dielectric properties of multiferroic $BiFeO_3$ nanoparticles synthesized by a novel citrate combustion method, Adv. Mat. Lett. 3(6), 533-538 (2012).
31. F. Huang, Z. Wang, X. Lu, J. Zhang, K. Min, W. Lin, R. Ti, T.-T. Xu, J. He, C. Yue, J. Zhu, Magnetism of $BiFeO_3$ nanoparticles. Peculiar with size approaching the period of the spiral spin structure, Sci. Rep. 3, 2907 (2013).
32. M. Hasan, M. A. Basith, M. A. Zubair, M. S.Hossain, R. Mahbub, M. A. Hakim, and M. F. Islam, Saturation magnetization and band gap tuning in $BiFeO_3$ nanoparticles via co-substitution of Gd and Mn, J. Alloys Compd. 687, 701-706 (2016).

33. T.Wang, T.Xu, S.Gao, and S-H. Song, Effect of Nd and Nb co-doping on the structural, magnetic and optical properties of multiferroic $BiFeO_3$ nanoparticles prepared by sol-gel method. Ceram. Int. 43, 4489-4495 (2017).
34 P.P. Khirade, S.D. Birajdar, A. B. Shinde, and K. M. Jadhav. Room temperature ferromagnetism and photoluminescence of multifunctional Fe doped $BaZrO_3$ nanoceramics. J. Alloys Compd. 691, 287-298 (2017).
35 C. Peng, X. Xu, C. Koenigsmann, A.C. Santulli, S.S. Wong, and J.L. Musfeldt, Size-dependent infrared phonon modes and ferroelectric phase transition in $BiFeO_3$ nanoparticles. Nano Lett. 10, 4526 (2010).
36 V. Annapu Reddy, N. P. Pathak, and R. Nath, Particle size dependent magnetic properties and phase transitions in multiferroic $BiFeO_3$ nano-particles. J. Alloys Compd. 543, 206 (2012)
37 X. Bai, J. Wei, B. Tian, Y. Liu, T. Reiss, N. Guiblin, P. Gemeiner, B. Dkhil, and I.C. Infante, Size effect on optical and photocatalytic properties in BiFeO3 nanoparticles, J. Phys. Chem. C 120, 3595-3601 (2016).
38 J. Hoon Jeon, H.-Y. Joo, Y.-M. Kim, D. Hyun Lee, J.-S.Kim, Y.S. Kim, T.Choi, and B.H. Park, Selector-free resistive switching memory cell based on $BiFeO_3$ nano-island showing high resistance ratio and nonlinearity factor, Sci. Rep. 6, 23299 (2016).
39. S. Hong, T. Choi, J.H. Jeon, Y. Kim, H. Lee, H.-Y. Joo, I. Hwang et al., Large Resistive Switching in Ferroelectric $BiFeO_3$ Nano-Island Based Switchable Diodes. Adv. Mater. 25, 2339-2343 (2013).
40. T. Sakamoto, K. Okada, A. N. Hattori, T. Kanki, A.S. Borowiak, B. Gautier, B. Vilquin, and H. Tanaka, Epitaxial inversion on ferromagnetic $(Fe, Zn)_3O_4$/ferroelectric $BiFeO_3$ core-shell nanodot arrays using three dimensional nano-seeding assembly. J. Appl. Phys. 113, 104302 (2013).
41. X. Zhang, B. Wang, X. Wang, X. Xiao, Z. Dai, W. Wu, J. Zheng, F. Ren, and C. Jiang, Preparation of M@$BiFeO_3$ Nanocomposites (M= Ag, Au) Bowl Arrays with Enhanced Visible Light Photocatalytic Activity. J. Am. Ceram. Soc. 98(7), 2255-2263 (2015).
42. M. Fiebig, Revival of the magnetoelectric effect, J. Phys. D: Appl. Phys. 38, R123 (2005).
43. N. A. Spaldin and M. Fiebig, Materials science. The renaissance of magnetoelectric multiferroics. Science, 309, 391-392 (2005).
44. J.M. Rondinelli, N.A. Spaldin, Structure and properties of functional oxide thin films: Insights from electronic-structure calculations. Adv. Mater., 23, 3363 (2011).
45. A. P. Pyatakov, A. K.Zvezdin, Magnetoelectric and multiferroic media, Phys. Usp. 55(6) 557 (2012).
46. J. F. Scott. Data storage: Multiferroic memories, Nat. Mater. 6, 256-257 (2007).
47. R. Ramesh & Nicola A. Spaldin, Multiferroics: progress and prospects in thin films, Nat. Mater. 6, 21-29 (2007).
48. P. Fischer, M. Polomska, I. Sosnowska, M. Szymanski, Temperature dependence of the crystal and magnetic structures of $BiFeO_3$, J. Phys. C: Solid St. Phys. 13, 1931-1940 (1980).
49. G. Catalan, J.F. Scott, Physics and Applications of Bismuth Ferrite, Adv. Mater. 21, 1–23 (2009).
50 F. Huang, Z. Wang, X. Lu, J. Zhang, K. Min, W. Lin, R. Ti et al. Peculiar magnetism of $BiFeO_3$ nanoparticles with size approaching the period of the spiral spin structure. Sci. Rep. 3, 2907 (2013).
51 S.M. Selbach, T. Tybell, M.-A. Einarsrud, and T. Grande. Size-dependent properties of multiferroic $BiFeO_3$ nanoparticles. Chem. Mater. 19, 6478-6484 (2007).

52 M.E. Castillo, V.V. Shvartsman, D. Gobeljic, Y. Gao, J. Landers, H. Wende and D. C. Lupascu, Effect of particle size on ferroelectric and magnetic properties of $BiFeO_3$ nanopowders. Nanotechnology 24, 355701 (2013).

53. A.N. Morozovska, E.A. Eliseev, M.D. Glinchuk, Ferroelectricity enhancement in confined nanorods: Direct variational method, Phys. Rev. B 73, 214106 (2006).

54 A.N. Morozovska, E.A. Eliseev. Surface and finite size effect on fluctuations dynamics in nanoparticles with long-range order. J. Appl. Phys. 107, 044101 (2010).

55 A.K. Tagantsev and G. Gerra, Interface-induced phenomena in polarization response of ferroelectric thin films, J. Appl. Phys. 100, 051607 (2006).

[56] Ivan S. Vorotiahin, Eugene A. Eliseev, Qian Li, Sergei V. Kalinin, Yuri A. Genenko and Anna N. Morozovska. Tuning the Polar States of Ferroelectric Films via Surface Charges and Flexoelectricity. Acta Materialia **137** (15), 85–92 (2017)

[57] Eugene A. Eliseev, Ivan. S. Vorotiahin, Yevhen M. Fomichov, Maya D. Glinchuk, Sergei V. Kalinin, Yuri A. Genenko, and Anna N. Morozovska. Defect driven flexo-chemical coupling in thin ferroelectric films. Physical Review **B, 97,** 024102 (2018)

[58] Eugene A. Eliseev, Yevhen M. Fomichov, Sergei V. Kalinin, Yulian M. Vysochanskii, Peter Maksymovich and Anna N. Morozovska. Labyrinthine domains on the phase diagram of ferroelectric nanoparticles: a manifestation of gradient-driven topological phase transition (http://arxiv.org/abs/1801.03545)

[59] A.N. Morozovska, E.A. Eliseev, Yulan Li, S.V. Svechnikov, P. Maksymovych, V.Y. Shur, Venkatraman Gopalan, Long-Qing Chen, and S.V. Kalinin,Thermodynamics of nanodomain formation and breakdown in Scanning Probe Microscopy : Landau-Ginzburg-Devonshire approach, Phys. Rev. B. 80, 214110 (2009).

[60] Shou-Ling Hou, and N. Bloembergen. "Paramagnetoelectric Effects in NiS O 4· 6 H 2 O." *Physical Review* 138, no. 4A: A1218 (1965).

[61]V. V. Shvartsman, S. Bedanta, P. Borisov, W. Kleemann, A. Tkach, and P. M. Vilarinho. "(Sr, Mn) TiO 3: A Magnetoelectric Multiglass." Physical review letters 101, no. 16: 165704 (2008).

[62]Barry, Howes, Marco Pelizzone, Peter Fischer, Cristobal Tabares-Munoz, Jean-pierre Rivera, and Hans Schmid. "Characterisation of some magnetic and magnetoelectric properties of ferroelectric Pb (Fe1/2Nb1/2) O3." *Ferroelectrics* 54, no. 1, 317-320 (1984).

[63]T. Watanabe, and K. Kohn. "Magnetoelectric effect and low temperature transition of PbFe0. 5Nb0. 5O3 single crystal." *Phase Transitions: A Multinational Journal* 15, no. 1: 57-68 (1989).

[64]W. Kleemann, V. V. Shvartsman, P. Borisov, and A. Kania. "Coexistence of antiferromagnetic and spin cluster glass order in the magnetoelectric relaxor multiferroic PbFe 0.5 Nb 0.5 O 3." *Physical review letters* 105, no. 25 (2010): 257202.

[65]Weiyang Wang, L-Q. Yan, J-Z. Cong, Y-L. Zhao, F. Wang, S-P. Shen, T. Zou, D. Zhang, S.-G. Wang, X.-F. Han, Y. Sun, Magnetoelectric coupling in the paramagnetic state of a metal-organic framework. Scientific Reports 3: paper ID 2024 (2013) DOI: 10.1038/srep02024.

[66] V.V. Laguta, A.N. Morozovska, E.A. Eliseev, I.P. Raevski, S.I. Raevskaya, E.I. Sitalo, S.A. Prosandeev, and L. Bellaiche. Room-temperature paramagnetoelectric effect in magnetoelectric multiferroics $Pb(Fe_{1/2}Nb_{1/2})O_3$ and its solid solution with $PbTiO_3$, J. Mater. Sci. 51, 5330-5342 (2016).

[67] S. Prosandeev, I.A. Kornev, L. Bellaiche, Magnetoelectricity in $BiFeO_3$ films: First-principles based computations and phenomenology, Phys. Rev. B 83, 020102 (2011).